ChemPubSoc Europe

DOI: 10.1002/cmdc.201900114

CHEMMEDCHEM Full Papers

Structurally Diverse Histone Deacetylase Photoreactive Probes: Design, Synthesis, and Photolabeling Studies in Live Cells and Tissue

Shaimaa M. Aboukhatwa,[a, b] Thomas W. Hanigan,[a] Taha Y. Taha,[a] Jayaprakash Neerasa,[a] Rajeev Ranjan,[c] Eman E. El-Bastawissy,[b] Mohamed A. Elkersh,[b, d] Tarek F. El-Moselhy,[b] Jonna Frasor,[e] Nadim Mahmud,[c] Alan McLachlan,[f] and Pavel A. Petukhov*[a]

Histone deacetylase (HDAC) activity is modulated in vivo by post-translational modifications and formation of multiprotein complexes. Novel chemical tools to study how these factors affect engagement of HDAC isoforms by HDAC inhibitors (HDACi) in cells and tissues are needed. In this study, a synthetic strategy to access chemically diverse photoreactive probes (PRPs) was developed and used to prepare seven novel HDAC PRPs **9**–**15**. The class I HDAC isoform engagement by PRPs was determined in biochemical assays and photolabeling experiments in live SET-2, HepG2, HuH7, and HEK293T cell lines and in mouse liver tissue. Unlike the HDAC protein abundance and biochemical activity against recombinant HDACs, the chemotype of the PRPs and the type of cells were key in defining the engagement of HDAC isoforms in live cells. Our findings suggest that engagement of HDAC isoforms by HDACi in vivo may be substantially modulated in a cell- and tissue-type-dependent manner.

Introduction

Histone deacetylases (HDACs) are promising therapeutic targets.[1] Four HDAC inhibitors (HDACi) of multiple class I and II HDACs are US Food and Drug Administration (FDA) approved for the treatment of T-cell lymphoma and multiple myeloma. Because HDAC isoforms deacetylate both histone and non-histone proteins and generally play unique non-redundant functions,[2] it is hypothesized that selective HDACi will offer a desired therapeutic effect while minimizing toxicity. To investigate this hypothesis, many isoform-selective HDACi have been synthesized and tested (Figure 1).[3]

HDACi potency and isoform selectivity are typically evaluated in biochemical assays under pseudo-equilibrium using individual purified recombinant HDAC isoforms and a synthetic substrate. However, substrate specificity and HDAC catalytic activity, and hence biological function, of HDACs are often modulated in vivo by the formation of protein–protein complexes and post-translational modifications,[4] which these assays do not recapitulate. It was also demonstrated that the catalytic activity of at least some of the HDACs is dispensable and HDACs can play a non-enzymatic structural (scaffolding) role.[2b] These modulatory mechanisms have been shown to be cell-state dependent and can be dysregulated in diseases and conditions.[5] A typical alternative approach in this case would be to use cellular phenotypic readouts. With few exceptions, HDAC isoform substrate specificity in live cells and in vivo is poorly understood, and these biochemical assays almost always remain the only avenue for measuring potency and selectivity of HDACi. HDACi are non-hydrolysable HDAC substrate analogues, and therefore, the same mechanisms that control the substrate specificity of HDACs should also affect the binding of HDACi. Because cellular context is lost in the biochemical inhibitory assays, HDACi potency and selectivity may not accurately reflect the in situ target engagement of HDACi. Several experimental approaches, including HDAC photoreactive probes (PRPs), have emerged to assess HDACi target engagement within complex systems.[6] The importance of cellular context to study the engagement of HDACs was further highlighted by a recent study by Bantscheff et al.,[6a] who showed that HDACi

[a] S. M. Aboukhatwa, Dr. T. W. Hanigan, T. Y. Taha, Dr. J. Neerasa, Prof. Dr. P. A. Petukhov
Department of Medicinal Chemistry and Pharmacognosy, College of Pharmacy, University of Illinois at Chicago, 833 South Wood Street, Chicago, IL 60612 (USA)
E-mail: pap4@uic.edu

[b] S. M. Aboukhatwa, Dr. E. E. El-Bastawissy, Dr. M. A. Elkersh, Prof. Dr. T. F. El-Moselhy
Department of Pharmaceutical Chemistry, Faculty of Pharmacy, Tanta University, Tanta, 31527 (Egypt)

[c] Dr. R. Ranjan, Prof. Dr. N. Mahmud
Section of Hematology/Oncology, College of Medicine, University of Illinois at Chicago, Chicago, IL 60612 (USA)

[d] Dr. M. A. Elkersh
Department of Pharmaceutical Chemistry, Faculty of Pharmacy, Pharos University, Alexandria 21311 (Egypt)

[e] Prof. Dr. J. Frasor
Department of Physiology and Biophysics, College of Medicine, University of Illinois at Chicago, Chicago, IL 60612 (USA)

[f] Prof. Dr. A. McLachlan
Department of Microbiology and Immunology, College of Medicine, University of Illinois at Chicago, Chicago, IL 60612 (USA)

Supporting information and the ORCID identification number(s) for the author(s) of this article can be found under: https://doi.org/10.1002/cmdc.201900114.

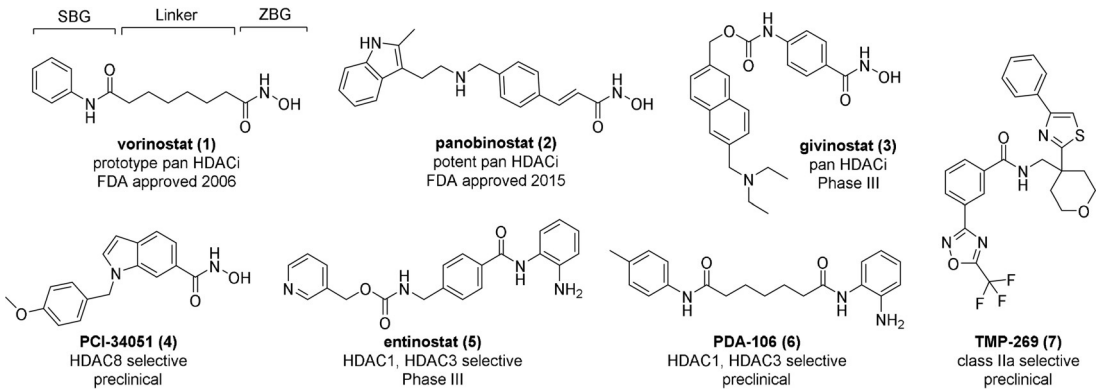

Figure 1. Representative HDACi **1**–**7** of diverse chemotypes in different stages of clinical development. The pharmacophore of HDACi is annotated on the structure of vorinostat (**1**). SBG: surface binding group, ZBG: zinc binding group.

tethered to polymer beads exhibited chemotype- and deacetylase-complex-dependent binding to HDAC isoforms. Cell-permeable HDAC PRPs were reported by Cravatt et al.,[6c,7] Storer et al.,[8] and our research group.[6f,9] Despite the overall progress in applying PRPs to study engagement of HDACs in situ, synthetic accessibility to drug-like cell-permeable HDAC PRPs with photoreactive groups able to generate short-lived reactive intermediates to accurately report on target engagement is limited.

We recently demonstrated that the incorporation of a photoreactive tetrafluorophenylazide (TFPA) group and an alkyne reporter into the surface binding group (SBG) results in a potent, relatively nonselective and cell-permeable photoreactive probe (**8**, Figure 2) that structurally resembles an FDA-approved HDACi (**1**, Figure 1).[6f] Photolabeling with this probe showed that engagement of HDAC isoforms depends on the post-translational modification state of HDACs, which is cell-type dependent and generally does not correlate with the selectivity profile measured in biochemical assays. The goal of the current study is to design and synthesize PRPs based on **1** and other common HDACi **2**–**7** (Figure 1) and validate them in target engagement studies in live cells in culture and in tissues in situ. To accomplish this goal, we developed a general synthetic strategy that incorporates a TFPA and alkyne reporter groups as an integral part of the SBGs of HDACi, designed and synthesized seven novel PRPs **9**–**15** (Figure 2), evaluated their biochemical potency and selectivity for individual recombinant HDAC isoforms, and conducted photolabeling studies in four cell lines in culture and in mouse liver tissue.

Results

PRP design and chemical synthesis

The PRPs synthesized in this work are based on diverse parent HDACi with varying ZBG, linker and SBG. Parent HDACi containing three ZBGs were chosen to synthesize PRPs **8**–**15**. These include either hydroxamic acid (**8**–**12**), *o*-aminoanilide (**13** and **14**), or trifluoromethyloxadiazole (**15**) (Figure 2). Linker regions of the PRPs contained both saturated and unsaturated aliphatic and aromatic moieties similar to those in the reported HDACi (Figure 1). Although several photoreactive groups are accessible synthetically, TFPA was chosen based on its similarity to aryl-based moieties present in the SBG of most HDACi, short half-life of the corresponding nitrene to capture interactions with HDACs (and possibly other proteins) while PRPs are still in the binding site of HDACs,[10] and fewer side-reactions that could decrease the yield of the PRP–protein adducts.[11] The alkyne handle was chosen because it is small, electronically inert, and stable in biological systems, yet reactive under copper(I)-catalyzed "click" reaction conditions. Given the extensive structure–activity relationships (SAR) available for most of the parent compounds, the TFPA and alkyne moieties were placed at positions deemed to tolerate the same size substituents when possible. The ZBG and linker regions were unaltered to maintain similarity to the parent HDACi.[12] All the parent HDACi and the corresponding PRPs were docked to the binding site of HDAC isoforms as described previously[13] to ensure that the TFPA and the reporter alkyne moieties do not interfere with the binding of the PRPs. The in silico physicochemical

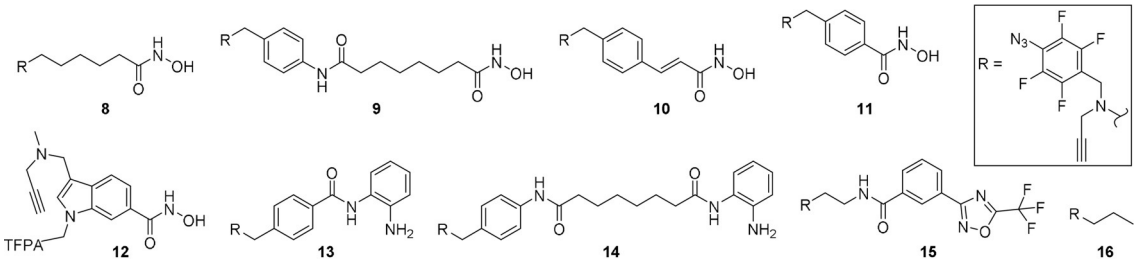

Figure 2. Tetrafluorophenylazide (TFPA) photoreactive probes **8**–**15** designed based on diverse chemotype HDACi and TFPA control compound **16**.

properties; octanol/water partition coefficient (Slog*P*), solubility (log*S*), and topological polar surface area (TPSA) of PRPs and the parent HDACi were calculated and compared with those of the parent HDACi (Figure S1 and Table S1 in the Supporting Information). Generally, the differences in Slog*P*, log*S*, and TPSA between the parent HDACi and PRPs were found to be similar to or smaller than those for the previously published PRPs.

PRPs **8** and **9** were designed based on the chemotype of **1** (Figure 1). PRP **8** isosterically replaces the phenyl ring of **1** with the TFPA and alkyne moieties so that only a single phenyl ring is present in the SBG. PRP **9** includes the TFPA and alkyne handle extended off the phenyl ring of **1**. PRP **10** was designed based on the chemotype of the potent pan-HDACi panobinostat, **2** (Figure 1) and its published SAR.[14] PRP **11** represents an aromatic hydroxamic acid class of HDACi similar to givinostat (**3**). The chemotype of HDAC8-selective compound PCI-34051 (**4**) was used to design PRP **12**. Replacement of the *p*-methoxyphenyl substituent at the indole nitrogen atom with the TFPA group and attachment of the alkyne handle at the indole C3 were chosen, as both positions could tolerate substituents of similar electronic and steric properties while retaining HDAC8 selectivity.[15] PRPs **13** and **14** were based on the *o*-aminoanilide-based inhibitors selective for HDAC1 and HDAC3,[16] entinostat (**5**) and PDA-106 (**6**), respectively. PRP **15** was designed by replacing the SBG of TMP-269 (**7**), a class-IIa-selective inhibitor,[17] with TFPA and alkyne moieties. Compounds **16** (Figure 2 and Scheme S1) and **S20** (Scheme S2) were designed to serve as a control for nonspecific photolabeling and as a competitor lacking the alkyne tag, respectively.

To incorporate the TFPA and alkyne moieties into a structurally diverse set of HDACi chemotypes, the synthetic strategy needed to be amenable to the reaction conditions used in the synthesis of the parent compounds. For example, most parent compounds use reductive amination for amine synthesis, hydroxylamine hydrochloride reaction with esters to form hydroxamic acid ZBG, or acid-catalyzed Boc deprotection to form benzamide ZBG. We found that TFPA was not stable in most of the standard reaction conditions used for the synthesis of the parent compounds (Scheme S3). To circumvent this issue, our optimized general strategy installs TFPA in the final steps of the synthesis from a perfluorobenzyl (PFB) group, in the presence of a protected ZBG. Further deprotection of the ZBG under mild conditions allows all the other moieties to remain intact. Our optimized general strategy for the synthesis of HDAC PRPs is outlined in Scheme 1 and detailed for PRPs **9**–**15** in Schemes 2–6. The synthetic schemes for the non-HDACi control **16** and the competitor **S20** are provided in Supporting Information Schemes S1 and S2, respectively.

The synthesis of PRPs **9** and **14** is shown in Scheme 2. A reductive amination reaction of pentafluorobenzaldehyde with *p*-(aminomethyl)aniline **17** gave secondary amine **18**. Coupling of suberic acid monomethyl ester with either *O*-tritylhydroxylamine **19** or *N*-boc-1,2-phenylenediamine **20** followed by ester hydrolysis gave acids **21** and **22**, respectively. Coupling of **18** with either **21** or **22** gave the secondary amines **23** and **24** that were alkylated with propargyl bromide resulting in **25** and **26**, respectively. The intermediates **25** and **26** were subject to regioselective azidation to yield the TFPA derivatives **27** and

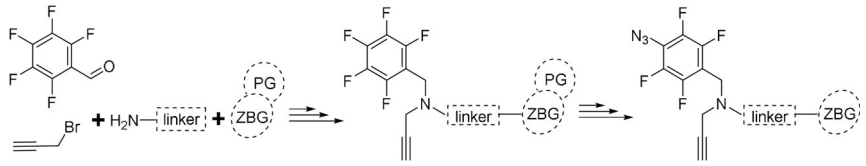

Scheme 1. General synthetic strategy for PRPs **8**–**15**. PG: protecting group.

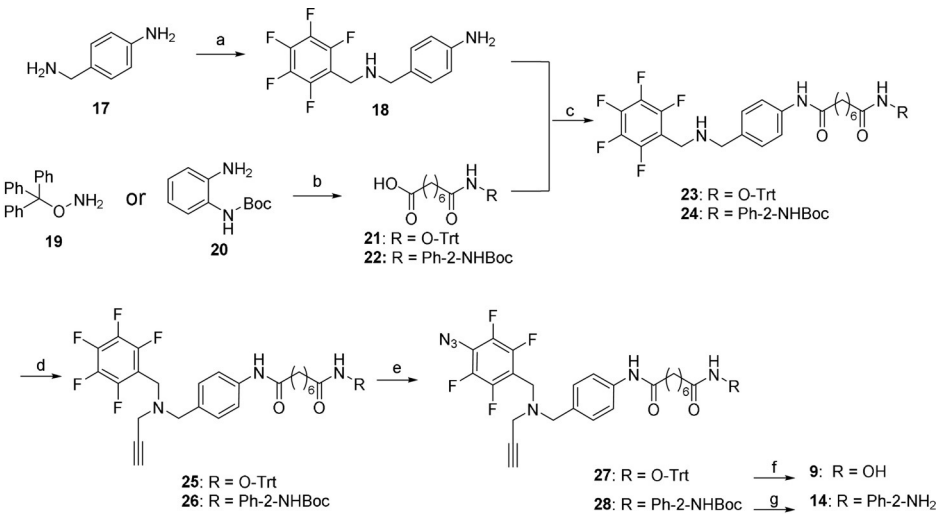

Scheme 2. Synthesis of PRPs **9** and **14**: a) 1. perfluorobenzaldehyde, CH_2Cl_2, 18 h, 2. $NaBH_4$, CH_3OH, 0 °C→RT, 4 h; b) 1. octanedioic acid monomethyl ester, EDC·HCl, HOBt, DMAP, Et_3N, $CHCl_3$, 18 h, 2. NaOH, 2:1 MeOH/H_2O, 8 h; c) EDC·HCl, HOBt, Et_3N, $CHCl_3$, 12 h; d) propargyl bromide, K_2CO_3, CH_3CN, 16 h; e) NaN_3, Bu_4NN_3, DMF, 75–80 °C, 18 h; f) $MgBr_2$, CH_2Cl_2, 30 min; g) HCl, 1,4-dioxane, 0 °C, 3 h.

28, respectively. Detritylation of **27** was carried out under mild Lewis-acid-catalyzed conditions to give PRP **9**. Deprotection of **28** under acidic conditions gave the *o*-aminoanilide PRP **14**.

As shown in Scheme 3, the synthesis of PRP **10** started with the procedure reported for its parent compound **2**.[14] The resulting aldehyde **31** was reacted with propargylamine under

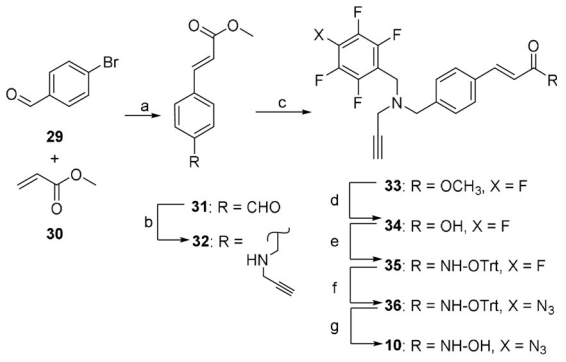

Scheme 3. Synthesis of PRP **10**: a) $Pd(OAc)_2$, NaOAc, NMP, 120 °C, 1 h; b) propargylamine, STAB-H, DCE, 16 h; c) perfluorobenzyl bromide, K_2CO_3, CH_3CN, 14 h; d) LiOH, 2:1 THF/H_2O, 20 h; e) **19**, EDC·HCl, HOBt, DMAP, Et_3N, $CHCl_3$, 6 h; f) NaN_3, Bu_4NN_3, DMF, 75–80 °C, 18 h; g) $MgBr_2$, CH_2Cl_2, 3 h.

reductive conditions to give **32**, which was alkylated with PFB bromide to give the amino ester **33**. A sequence of hydrolysis, tritylation, azidation, and deprotection yielded the final PRP **10**. The synthesis of PRPs **11** and **13** is shown in Scheme 4. Re-

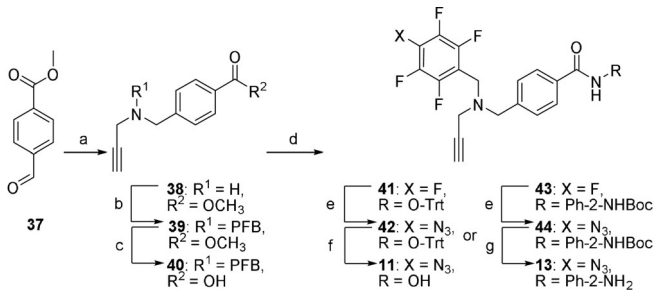

Scheme 4. Synthesis of PRPs **11** and **13**: a) 1. propargylamine, CH_2Cl_2, 16 h, 2. $NaBH_4$, CH_3OH, 0 °C→RT, 4 h; b) pentafluorobenzyl bromide, K_2CO_3, CH_3CN, 16 h; c) LiOH, 6:3:1 THF/H_2O/dioxane, 24 h; d) **19** for **41** or **20** for **43**, EDC·HCl, HOBt, DMAP, Et_3N, $CHCl_3$, 12 h; e) NaN_3, Bu_4NN_3, DMF, 75–80 °C, 18 h; f) $MgBr_2$, CH_2Cl_2, 3 h; g) HCl, 1,4-dioxane, 0 °C, 6 h. PFB: perfluorobenzyl.

ductive amination of methyl 4-formylbenzoate **37** with propargyl amine gave the secondary amine **38** that was alkylated with PFB bromide and hydrolyzed to the corresponding acid **40**. Coupling of acid **40** with either **19** or **20** followed by azidation and deprotection gave PRPs **11** and **13**, respectively. PRP **12** was synthesized as shown in Scheme 5. Alkylation of the N-1 nitrogen atom of the commercially available indole **45** followed by reductive amination with *N*-methyl propargyl amine gave ester **47**. Hydrolysis of **47** followed by reaction with **19** resulted in ester **49** that was subjected to azidation and deprotection to give PRP **12**. The synthesis of PRP **15** is shown in

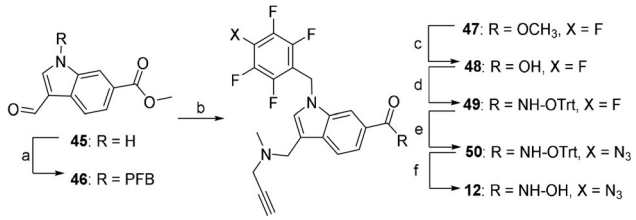

Scheme 5. Synthesis of PRP **12**: a) perfluorobenzyl bromide, NaH, DMF, 14 h; b) *N*-methylpropargylamine, STAB-H, DCE, 5 h; c) LiOH, 6:3:1 THF/H_2O/dioxane, 12 h; d) **19**, EDC·HCl, HOBt, DMAP, Et_3N, $CHCl_3$, 6 h; e) NaN_3, Bu_4NN_3, DMF, 50 °C, 22 h; f) $MgBr_2$, CH_2Cl_2, 3 h. PFB: perfluorobenzyl.

Scheme 6. Trifluoromethyloxadiazole **53** was synthesized following a previously reported procedure.[17] The perfluorophenyl group and the alkyne moieties were reacted with ethylene diamine **54** via reductive amination followed by alkylation to give **58**. Next, coupling of **53** and **58**, followed by azidation gave the final product **15**.

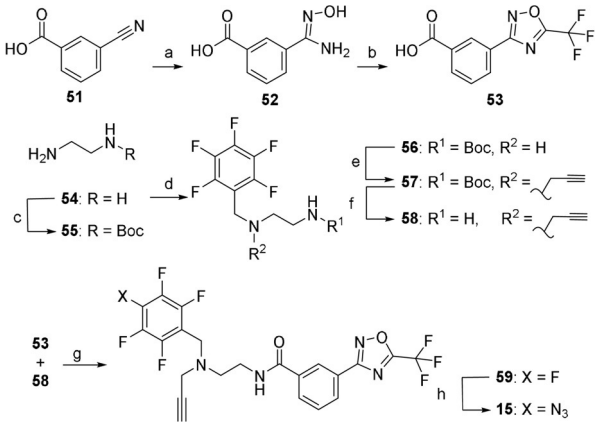

Scheme 6. Synthesis of PRP **15**: a) NH_2OH, Na_2CO_3, 1:1 MeOH/H_2O, Reflux, 4 h; b) trifluoroacetic anhydride, 0→50 °C, pyridine, 5 h; c) $(Boc)_2O$, $CHCl_3$, 0 °C→RT; d) 1. perfluorobenzaldehyde, CH_2Cl_2, 8 h, 2. $NaBH_4$, CH_3OH, 0 °C→RT, 3 h; e) propargyl bromide, K_2CO_3, CH_3CN, 48 h; f) HCl, 1,4-dioxane, 1 h; g) EDC·HCl, HOBt, DMAP, Et_3N, $CHCl_3$, 12 h; h) NaN_3, Bu_4NN_3, DMF, 80 °C, 18 h.

As mentioned above, azidation of the PFB group was performed near the end of each synthesis, as the resulting arylazido TFPA group was found to be unstable under the reaction conditions typically used to prepare most of the parent HDACi. Specifically, we found that the TFPA group could not withstand conditions necessary for reductive amination, palladium-catalyzed cross-coupling, and reactions of hydroxylamine hydrochloride under basic conditions including amidoxime formation from nitriles and hydroxamic acid formation from esters. Several rounds of experimentation with different conditions and synthetic routes showed that coupling of the corresponding carboxylic acid with *O*-trityl hydroxylamine permitted the introduction and maintenance of the masked hydroxamic acid ZBG during all the steps of the synthesis (Scheme S3 A). Azidation of the PFB group with trimethylsilyl azide resulted in low yields of the desired TFPA product, regardless of temperature, solvent, and reaction duration. It was found that the reaction

between PFB-based intermediates and stochiometric amounts of sodium azide and catalytic amounts of tetrabutylammonium azide, which was adopted from previously reported procedure,[18] gave 25–95% yields. The temperature and reaction time needed optimization for each chemotype to ensure complete conversion of PFB to TFPA. It was also important to monitor completion of the reaction using liquid chromatography–mass spectrometry analysis (LC–MS) and ^{19}F NMR, as the starting PFB derivatives often exhibited identical retention times and were inseparable by chromatography. Lowering the reaction temperature required longer reaction times, resulting in the formation of additional side products and decreased yield. The optimal temperature and duration of this reaction were ~80 °C and ~18 h, respectively, except for intermediate **50**, for which this reaction had to be conducted at 50 °C for 22 h to obtain acceptable (≥25%) reaction yields (Scheme S3C).

For hydroxamate PRPs, detritylation of intermediates **27**, **36**, **42**, and **50** (Schemes 2–5) was carried out using a Lewis-acid-mediated deprotection.[19] Protic acids commonly used for deprotection, such as trifluoroacetic acid and hydrochloric acid, were found to be incompatible in deprotection of intermediates containing a TFPA moiety, resulting in a complex mixture of products (Scheme S3D). Deprotection of Boc intermediates **28** and **44** (Schemes 2 and 4) required an ice-cooled reaction for 3–6 h. Longer reaction times or reactions at room temperature gave the previously reported benzimidazole cyclization side product as detected by LC–MS (Scheme S3E).[20]

It is also important to note that mild hydrolysis conditions, LiOH in THF/water at room temperature, were used for the hydrolysis of PFB esters **33**, **39**, and **47**, whereas methyl esters of **21** and **22** were hydrolyzed with NaOH in methanol/water. The latter conditions in the case of **33**, **39**, and **47** or heating above 40 °C resulted in *para*-hydroxylated PFB side products (as detected by LC–MS and NMR) that were inseparable from the desired products in the subsequent reaction steps (Scheme S3B).

Biochemical selectivity

The PRPs and their parent compounds were tested for HDAC inhibitory activity against recombinant class I HDACs as well as HDAC4, as a representative member of class II isoforms, using a standard experimental procedure with a competitive fluorescence-based assay commonly used in the field.[21] Briefly, inhibition of HDAC1, 2, and 3 was measured using the fluorescent HDAC substrate Boc-L-Lys(Ac)-AMC and commercially available recombinant human HDAC1, 2, and 3, whereas inhibition of HDAC8 was measured using the BML-KI178 HDAC8 substrate and a recombinant human HDAC8.[22] The pIC_{50} values for PRPs **8**–**15** relative to their parent HDACi **1**–**7**, are listed in Table 1 and their HDAC isoform selectivity profile is given in Table 2. The dose–response curves for all tested compounds are shown in Figure S2. The potency of PRPs was generally 10- to 100-fold lower than that of their parent compounds (Table 1), whereas the isoform selectivity profile of PRPs was similar, and in one case—PRP **13**—HDAC3 selectivity was superior to that of its parent HDACi **5** (Table 2).

PRP **8**, with high similarity to the structure of its parent HDACi **1**, showed the highest potency among all the PRPs, with pIC_{50} values of 6.3, 6.8, 7, and 5.6 against HDAC1, HDAC2, HDAC3, and HDAC8, respectively (Table 1). PRP **9** was about three-fold less potent than PRP **8** against all tested isoforms, with respective pIC_{50} values of 6.1, 6.0, 6.5, and 5.3 against HDAC1, HDAC2, HDAC3, and HDAC8 (Table 1). PRP **10**, with pIC_{50} ~5.5 for HDACs 1–3, was 10-fold less potent than PRPs **8** and **9** and 10000-fold less potent than the parent HDACi **2**, which exhibited pIC_{50} ~9.5 for HDACs 1–3. The potency of **10** against HDAC8, pIC_{50} = 5.1, was similar to those of **8** and **9** and was 19-fold lower than that of **2**: pIC_{50} = 6.4 (Table 1). PRP **11**, with an average pIC_{50} of ~5.0, was 30-fold less potent than the parent HDACi **3**, whose average pIC_{50} was ~6.5 against class I HDAC isoforms (Table 1). PRPs **8**–**11** showed little to no selectivity for any class I HDAC isoforms (Table 2).

Table 1. Biochemical pIC_{50} values of PRPs and their parent HDACi for HDAC1, 2, 3, 8 and 4.

Compound	$pIC_{50} \pm SE$[a]				
	HDAC1	HDAC2	HDAC3	HDAC8	HDAC4
vorinostat (**1**)	7.67 ± 0.01	6.92 ± 0.02	7.74 ± 0.02	6.61 ± 0.06	NA[b]
PRP **8**	6.26 ± 0.04	6.77 ± 0.04	6.96 ± 0.06	5.64 ± 0.11	4.42 ± 0.07
PRP **9**	6.13 ± 0.07	5.95 ± 0.08	6.46 ± 0.10	5.30 ± 0.10	NA[b]
panobinostat (**2**)	9.52 ± 0.10	9.70 ± 0.46	9.20 ± 0.20	6.41 ± 0.20	NA[b]
PRP **10**	5.56 ± 0.07	5.32 ± 0.05	5.69 ± 0.06	5.12 ± 0.09	NA[b]
givinostat (**3**)[23]	6.70[c]	6.49[c]	6.80[c]	6.07[c]	NA[b]
PRP **11**	5.43 ± 0.09	4.77 ± 0.01	4.96 ± 0.02	5.10 ± 0.06	NA[b]
PCI-34051 (**4**)	5.50 ± 0.08	4.60 ± 0.03	4.94 ± 0.04	8.48 ± 0.06	NA[b]
PRP **12**	3.33 ± 0.14	4.19 ± 0.06	5.30 ± 0.03	5.67 ± 0.08	NA[b]
entinostat (**5**)[24]	6.61[c]	6.34[c]	6.61[c]	< 5[c]	NA[b]
PRP **13**	5.09 ± 0.09	5.10 ± 0.12	5.82 ± 0.08	< 3	NA[b]
PDA-106 (**6**)	6.33 ± 0.07	6.54 ± 0.05	7.66 ± 0.02	5.24 ± 0.09	NA[b]
PRP **14**	3.91 ± 0.05	3.37 ± 0.11	5.43 ± 0.08	< 3	NA[b]
TMP-269 (**7**)	4.33 ± 0.10	4.44 ± 0.11	4.24 ± 0.07	< 3	4.54 ± 0.11
PRP **15**	3.95 ± 0.14	4.21 ± 0.04	< 3	2.81 ± 0.43	3.40 ± 0.78

[a] pIC_{50} is equal to (- log IC_{50}) and SE is standard error, both were calculated by nonlinear regression analysis (enzyme-inhibitor model) using GraphPad prism 7.02. Values reported are the mean ± SE at least 2 replicate experiments; the numbers are rounded to three significant figures. [b] NA: less than 50% inhibition at 100 μM. The percent of inhibition at 10 and 100 μM is given in Table S2. [c] pIC_{50} of both 5 and 6 were calculated based on reported biochemical inhibition data for both using similar assay in the annotated references.

Table 2. Biochemical selectivity profiles for PRPs **12**–**15** and their parent HDACi (**4**–**7**).

Compound	Selectivity[a]					
	HDAC1/HDAC2	HDAC1/HDAC3	HDAC1/HDAC8	HDAC2/HDAC3	HDAC2/HDAC8	HDAC3/HDAC8
vorinostat (**1**)	5.6	0.85	11	0.15	2.0	13
PRP **8**	0.31	0.20	4.2	0.65	13	21
PRP **9**	1.5	0.47	6.8	0.31	4.5	14
Panobinostat (**2**)	0.66	2.1	1300	3.2	1900	620
PRP **10**	1.7	0.74	2.8	0.43	1.6	3.7
givinostat (**3**)	1.6	0.79	4.3	0.49	2.6	5.4
PRP **11**	4.6	3.0	2.1	0.65	0.47	0.72
PCI-34051 (**4**)	7.9	3.6	0.0010	0.46	0.00013	0.00029
PRP **12**	0.14	0.011	0.0046	0.078	0.033	0.43
entinostat (**5**)	1.9	1.0	>40[b]	0.54	>22[b]	>41[b]
PRP **13**	0.98	0.19	>120[b]	0.19	>130[b]	>660[b]
PDA-**106** (**6**)	0.62	0.047	12	0.076	20.0	260
PRP **14**	3.5	0.030	>8.1[b]	0.0087	>2.3[b]	>270[b]
TMP-**269** (**7**)	0.78	1.2	>21[b]	1.6	>28[b]	>17[b]
PRP **15**	0.55	>8.9[b]	14	>16[b]	25	1.6

[a] Selectivity ratios based on IC50 measurements; values are rounded to two significant figures. [b] An estimate based on the highest concentration tested.

PRP **12** was 200-, 30-, and 2-fold more selective for HDAC8 (Table 2) with a pIC_{50} value of 5.7 as compared with pIC_{50} of 3.3, 4.2, and 5.3 for HDAC 1, 2, and 3, respectively (Table 1). PRPs **13** and **14** did not inhibit HDAC8 at the maximum tested concentration, 1 mM (Table 1). PRP **13** exhibited pIC_{50} values of 5.1, 5.1, and 5.8 for inhibition of HDAC1, 2, and 3, respectively (Table 1). PRP **14** had pIC_{50} values of 3.9, 3.4, and 5.4 against HDAC1, HDAC2, and HDAC3, respectively (Table 1). PRP **13** was 15-, 50-, and 3-fold more potent than **14** against HDACs 1, 2, and 3, respectively. Both PRPs **13** and **14** showed selectivity for HDAC3 over HDAC1 and HDAC2, higher than that of their respective parent HDACi **5** and **6** (Table 2). We found that both PRP **15** and its parent HDACi **7**, which was previously reported as being selective for class II HDACs,[17] were not selective for the class II HDAC4 and were generally weak inhibitors of all the tested isoforms, with pIC_{50} values ranging between 3 and 4 for both compounds (Table 1). The latter finding highlights the variability in the results of the biochemical assays usually encountered due to differences in experimental conditions.

In-cell photoaffinity labeling

Following our previously published procedure[6f] outlined in Figure 3, photolabeling experiments were performed in live SET-2 (Figure 4), HepG2, HuH7, and HEK293T cells (Figure 5). Corresponding densitometric analysis of selected class I HDAC labeling is given in Figures S3 and S4. Briefly, cells in culture were incubated with either DMSO or compound **16** as a control, PRP or a competitor HDACi and PRP and incubated for 40 min with PRPs **8**–**12** and **15** or for 3 h with PRPs **13** and **14**, irradiated with UV light at 366 nm, washed, and lysed. The labeled lysate was subjected to "click" reaction conditions with an azide-conjugated 800CW IRDye and electrophoretically separated. Antibodies for individual HDAC isoforms were added followed by incubation with 680RD IRDye conjugated secondary antibodies. Visualization in both 800 and 700 nm channels show PRP-labeled proteins as well as HDAC-antibody-bound proteins, respectively. The PRP-labeled bands (800 nm), which were absent from the controls and decreased by at least half upon addition of a competitor, were considered specific. These bands (800 nm) were assigned to a particular HDAC isoform if they counter-stained with an HDAC antibody (700 nm; Figure 3). The concentration of PRPs was optimized to achieve the highest signal-to-noise ratio (Figures S5 and S6) and was kept within the HDACi concentration range commonly used in cell-based studies[15,25] and typically observed in cancer patients undergoing HDACi-based therapy.[26]

In SET-2 cells, the bands observed with TFPA control compound **16** were the same as those observed with the DMSO control (Figures 4a and 4b), indicating that the TFPA moiety itself would have little effect on the labeling with PRPs. Labeling of HDAC8 was difficult to interpret due to a nonspecific band found in the control lanes at the same level as HDAC8 in SET-2 cells (Figure 4a). PRP **9**, which is a relatively potent inhib-

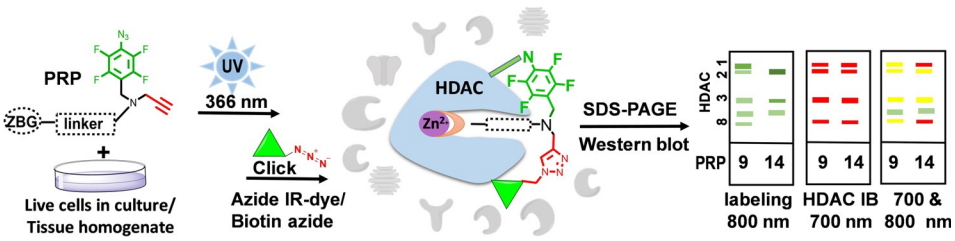

Figure 3. Experimental workflow of photoaffinity labeling in live cells and gel-based visualization of labeled proteins.

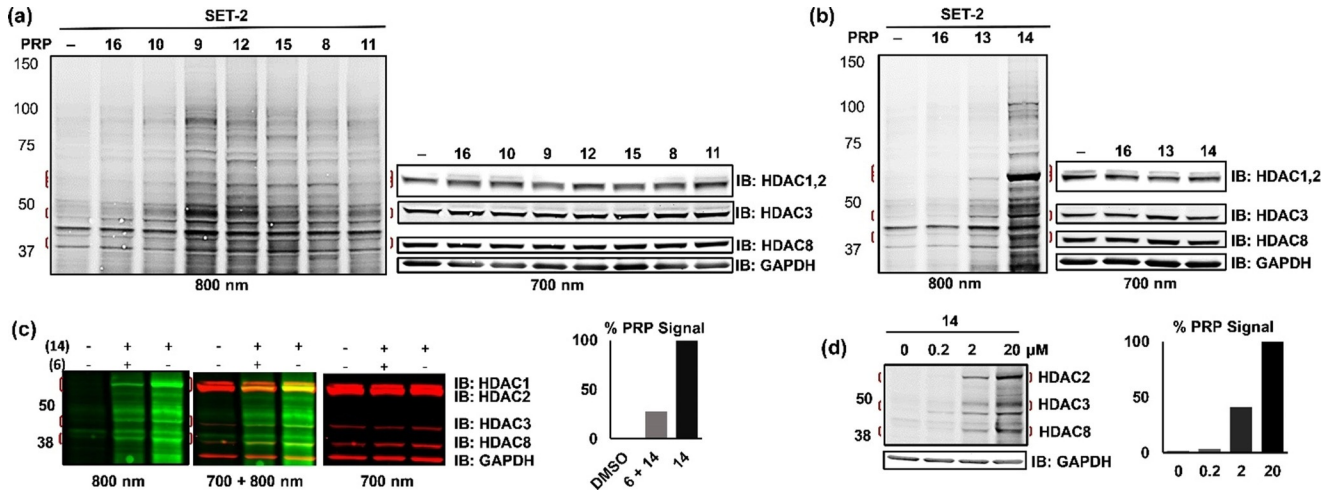

Figure 4. Photolabeling with PRPs **8**–**15** in live SET-2 cells. Labeling with (a) hydroxamate PRPs **8**–**12** and TFMO PRP **15**, (b) *o*-aminoanilide PRPs **13** and **14**. In each of (a) and (b), vehicle DMSO (–) and **16** were included as controls for nonspecific bands. (c) Competition of **14** HDAC-labeled bands with the HDACi **6**. (d) Concentration-dependent labeling of HDACs by **14**. In (c) and (d), densitometry of HDAC2 labeling bands normalized to HDAC2/GAPDH signal is shown to the right of each gel.

itor of all class I HDACs (pIC_{50} ~6), showed labeling of HDACs 1–3 higher than that observed with **8** (Figure 4a and Figure S3a). PRPs **10** and **11** showed weak labeling of HDAC1 and 2 isoforms only marginally different from the control (Figure 4a and Figure S3a). The HDAC8-selective PRP **12** showed weak labeling of HDAC1 and 2 and distinct labeling of HDAC3. Despite being a weak HDAC inhibitor in biochemical assays, PRP **15** labeled HDAC2 and 3, but not HDAC4, in live cells (Figure 4a and Figure S3a). The absence of HDAC4 labeling is likely due to the low abundance of HDAC4, as we could not detect it by HDAC4-specific antibody in this cell type. Unexpectedly, both HDAC3-selective PRPs **13** and **14** labeled mostly HDAC2, and to a lesser extent HDAC3 (Figure 4b and Figure S3b). Labeling of HDAC1 was indistinguishable from background. The labeling bands of HDAC2 and HDAC3 by PRP **14** were further confirmed by competition with the parent HDACi **6** (Figure 4c). PRP **14**, although being a relatively weak HDAC2 inhibitor in the biochemical assay (pIC_{50} = 3.4), labeled HDAC2 even at concentrations as low as 200 nM (Figure 4d). In preliminary labeling experiments using recombinant HDAC1 (Figure S7), co-incubation with the covalent competitor **S20** showed a ~75% decrease in labeling with PRP **8** relative to a 25% decrease when co-incubated with **1**. In live SET-2 cells, however, cellular levels of HDACs 1–3 and 8 were decreased upon co-treatment with **S20**, and both **S20** and **1** had a comparable 50% decrease in labeling of HDAC2 with PRP **8** (Figure S7).

Photolabeling of **9** and **14** was further characterized in HepG2, HuH7, and HEK293T cells (Figure 5). In HepG2 (Figure 5a and Figure S4a) and HuH7 (Figure 5b and Figure S4b), labeling patterns were similar to those observed in SET-2 cells for both **9** and **14**, with higher labeling of HDAC2 for PRP **14**. In HEK293T (Figure 5c and Figure S4c), **14** maintained its superior labeling of HDAC2, but to a lesser extent than in HepG2 and HuH7 cells. Labeling of HDAC1 in HEK293T was observed with both **9** and **14**. Immunoblotting with anti-HDAC1 and 2 antibodies showed only minor differences in the protein abundance in SET-2, HepG2, HuH7 and HEK293T cells, which does not explain the decreased labeling of HDAC2 by **14** in HEK293T cells (Figure S8).

In-tissue photoaffinity labeling

To investigate the feasibility of labeling HDACs with TFPA PRPs in tissues, PRP **8** was incubated with mouse liver homogenate, and the PRP-labeled lysates were subject to photolabeling in a workflow similar to that optimized for live cells in culture

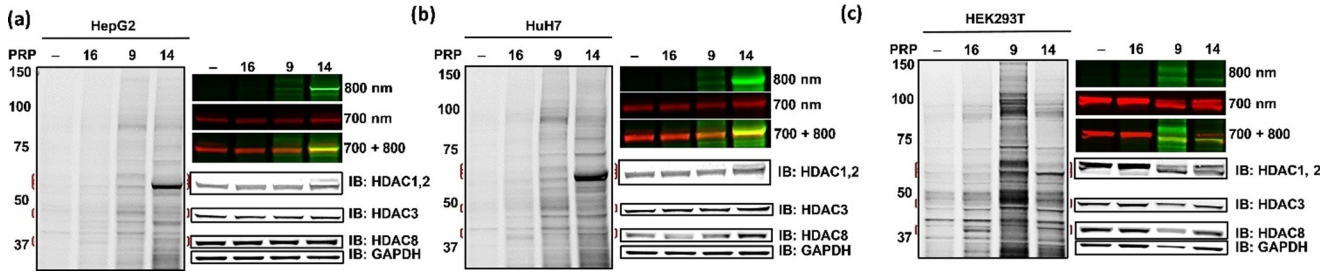

Figure 5. Photolabeling with PRPs **9** and **14** in (a) HepG2, (b) HuH7, and (c) HEK293T live cells. DMSO (–) and TFPA **16** were included as controls. IB with class I HDAC antibodies and GAPDH is shown to the right at the level of molecular weight for each protein. The top right part of each panel shows detection of HDAC2 labeling by IR dye (800 nm) and HDAC2 antibody (700 nm) and overlap of both labeling band and antibody (700 + 800 nm).

(Figure 3). Briefly, minced fresh mouse tissue was incubated with either DMSO or PRP **8** or pre-treated with **1** and then incubated with **8** and irradiated with 366 nm UV light. The amount of tissue was optimized to enable detection of class I HDAC isoforms. The labeled tissue was lysed, and the resulting lysate was reacted with the azide-conjugated biotin tag. The PRP-labeled bands were detected by 800CW IRDye-conjugated streptavidin. HDAC-specific labeling bands were absent from DMSO control, decreased by competition with **1** and counterstained with HDAC-specific antibodies (Figure 6 and Figure S9). The band corresponding to HDAC8 and recognized with an anti-HDAC8 was relatively low in intensity compared with that in experiments with live cells. We attribute this to the use of anti-HDAC8 antibody raised against human HDAC8. PRP **8** labeled HDAC1–3 and 8, with the most pronounced bands for HDAC8 (Figure 6 and Figure S9).

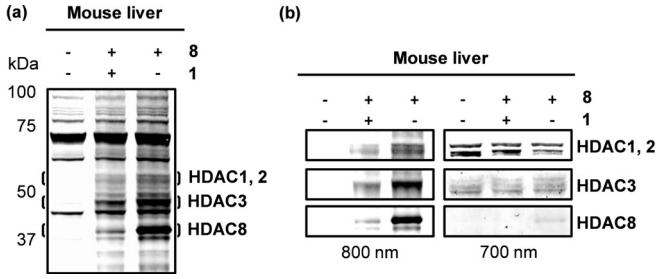

Figure 6. (a) Photolabeling with PRP **8** in mouse liver tissue, reacted with azide-conjugated biotin and incubated with 800CW IRDye-conjugated streptavidin. (b) Left: HDAC labeling bands as visualized in panel (a), right: immunoblotting with 680RD IRDye conjugated HDAC1, 2, 3, and 8 antibodies.

Discussion

HDAC isoform engagement with HDACi is an important issue in the development of HDAC-based therapeutics. It still needs a robust and readily implemented solution in typical biological settings and models. In this study, we have designed and synthesized a series of novel HDAC PRPs (Figure 2) based on known HDACi (Figure 1) with diverse chemotypes and biochemical selectivity profiles. To ensure structural and chemical uniformity and direct systematic comparison of different chemotypes, the same photoreactive group and reporter handle were used for all PRPs in this study. We also developed a synthetic strategy that is compatible with the TFPA photoreactive moiety and other groups in the pharmacophore of HDACi (Scheme 1) that, we anticipate, will enable others to access an even broader set of HDAC PRPs for target engagement studies.

We found that the convergent minimalistic synthetic approach described herein resulted in the expected PRPs in overall acceptable yields with an individual yield for each reaction throughout the synthesis of at least 25%, which is important for scaling up the synthesis of the PRPs. In the optimized synthetic scheme, unmasking of the photoreactive moiety was postponed to the last step to avoid the formation of side-products or losing the target compounds completely. Although PRPs containing TFPA and other azide-based photoreactive groups are typically stable in the dark below 0 °C for several weeks to a few months, they degrade upon prolonged storage. The ability to store a stock of non-photoreactive intermediates that can be readily converted in to PRPs in a few straightforward experimental steps is expected to prevent the loss of PRP during storage and to yield consistent results in photolabeling experiments. The overall applicability of this synthetic strategy was demonstrated with three different ZBGs, two of which can be found in the majority of HDACi in current use. Although further SAR studies may be needed, the convergent approach developed here can be used to conduct the necessary optimization as well as to extend this strategy to other not yet explored HDACi chemotypes.

The incorporation of the photoreactive and reporter handle groups resulted in a variable moderate decrease in potency of the resulting PRPs relative to their parent HDACi. The biochemical activity of the PRPs against HDACs 1–3 and 8 was between 125 nM and 1 mM (Table 1), and the selectivity was similar to that of the parent HDACi (Table 2). In general, PRPs **8**–**15** displayed robust labeling of class I HDAC isoforms in cells in culture. Among all the PRPs tested, PRP **14** showed the best signal-to-noise ratio and was able to detect HDAC2 in SET-2 cells even at 200 nM (Figure 4d). We also demonstrated that PRP **8** can label class I HDAC isoforms in mouse liver tissue. To the best of our knowledge, this is the first published example of labeling HDACs in tissue with a small-molecule-based PRP. Unlike other approaches commonly used in biology to study HDAC engagement, the application of PRPs is faster, inexpensive, and, most importantly, can be done in the commonly used biological models without modifications. Our studies were conducted in live cells in culture without overexpression of HDACs, suggesting that the sensitivity of the newly designed PRPs and photolabeling approach in general are sufficient to detect endogenous levels of HDACs in cells with unaltered machinery. This would be particularly useful for situations in which molecular biological manipulations with the cellular machinery are experimentally or methodologically undesirable or impossible.

The differences between the biochemical and cell-based photolabeling selectivity are observed for all the PRPs in this study. Our analysis shows that there are four types of differences. In the first type, less potent in biochemical assays PRPs **9** and **14** display higher labeling of HDACs than more potent congeners, **8** and **13**, respectively (Figures 4a and 4b and Figure S3). In the second type, the isoform selectivity patterns of PRPs **12**–**15** determined in the biochemical assays do not match those observed by photolabeling in live cells. For instance, PRP **14**, despite selectivity for HDAC3 in the biochemical assay (Table 2), showed pronounced labeling of HDAC2 in SET-2 (Figure 4b and Figure S3b), HepG2 (Figure 5a and Figure S4a), and HuH7 (Figure 5b and Figure S4b) cells. In the third type, the same PRPs targeted different HDAC isoforms in a cell-type-dependent manner. For example, PRR **14** showed higher HDAC2 labeling in HepG2 and HuH7 cells (Figures 5a and 5b) than that in HEK293T cells (Figure 5c), which could not be explained by the difference in isoform abundance (Fig-

ure S8). Whether this is due to the higher activity of HDAC2 in HepG2 and HuH7 cell lines[27] and the activity of HDAC1 being higher or equal to that of HDAC2 in the HEK293T cell line[2a,28] remains to be investigated. In the fourth type, the chemotype-dependent labeling profile was observed for PRPs of different ZBGs, *o*-aminoanilides **13** and **14** (Figure 4b, and Figure S3b) versus hydroxamates **8**–**12** (Figures 4a and Figure S3a). Regardless of the variability in the labeling pattern within each class, the overall labeling trend is characteristic of each ZBG chemotype. The hydroxamate-based PRPs **8**–**12** display a variable but consistent ability to label HDACs 1–3 and 8, whereas *o*-aminoanilide-based PRPs **13** and **14** labeled mostly HDAC2, to lesser extent HDAC3, and did not label HDAC1, the binding site of which is highly homologous to those of HDAC2 and HDAC3. This chemotype dependence of target engagement is consistent with the observations by Bantscheff et al.[6a] and may be linked to the slow k_{off} binding kinetics of the *o*-aminoanilide-based HDACi.[29] Although our efforts in this study were focused on the validation of photolabeling using class I HDACs, differences between the photolabeling and the biochemical profiles are expected for class II and IV HDACs as well. The overall discordance between the biochemical and cell-based relative selectivity is consistent with that recently demonstrated by us for PRP **8** in photolabeling of all zinc-dependent HDAC isoforms in different types of breast cancer cells.[6f] These findings further underscore the importance of the cellular context for target engagement.

This study shows that the observed differences between the biochemical and photolabeling profiles is a common phenomenon that does not depend on the abundance of the HDAC proteins, and the biochemical potency of PRPs and is primarily driven by the chemotype of the PRP and the type of cells. By comparing the labeling of HDAC isoforms in different cell lines by the same PRP, we can exclude the differences in binding conformations, yields in click reactions, and differences in photoactivation as factors for the discordance between the biochemical and the HDAC photolabeling profiles. Therefore, it can be argued that the cellular context affects photolabeling by PRPs, and more importantly HDAC isoform target engagement by HDACi, in several ways: 1) by altering the binding affinity and kinetics of the PRPs to HDACs via PTMs and/or conformational/accessibility changes due to multiprotein complex formation, and/or 2) by varying the relative abundance of the catalytically competent and catalytically inactive, for example, scaffolding, HDACs (Figure 7). Both these scenarios individually or in combination would present themselves in the same way in the photolabeling experiments in live cells. Although we cannot exclude either of these scenarios, this report clearly demonstrates that the answer to the question "What HDAC isoform(s) does this HDAC ligand inhibit in cells/in vivo?" is not straightforward and that HDAC PRPs would be a useful tool to address it. We anticipate that the differences between the biochemical profiles and the HDAC isoform engagement in live cells, as determined by the PRPs, should also be observed for the non-photoreactive parent HDACi, and should be taken into consideration when analyzing the outcomes of ongoing clinical trials of isoform-selective HDACi.[30] Further studies of the phenomenon observed here may lead to exciting new discoveries in the biology of HDAC and novel inhibitors with potency and selectivity engineered to be cell-type selective.

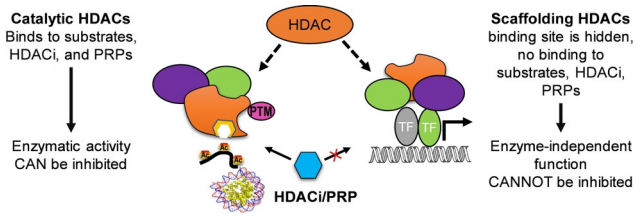

Figure 7. Hypothesis: Unlike scaffolding HDACs, catalytically active HDACs are able to bind substrates, small-molecule HDACi, and HDAC PRPs. PTMs and HDAC protein complex components define whether the role of HDAC isoform is catalytic or scaffolding in a cell-type, cell-cycle, and subcellular location manner.

Conclusions

In summary, a synthetic strategy to access diverse HDAC PRPs was developed. Novel HDAC PRPs **9**–**15** based on seven HDACi with diverse chemotypes **1**–**7** and biochemical selectivity profiles were synthesized, tested in HDAC1–3, 4, and 8 biochemical assays, and validated in photolabeling experiments in live SET-2 cells. In addition, photolabeling with PRPs **9** and **14** was also validated in HepG2, HuH7, and HEK293T cell lines, whereas PRP **8** was also tested for photolabeling capacity in mouse liver tissue. The synthetic strategy should be readily amenable for the synthesis of PRPs with chemotypes of other HDACi. In general, the HDAC biochemical selectivity profiles of PRPs were similar to those of their parent HDACi. The cell-based photolabeling and biochemical profiles of PRPs **9**–**15** were found to be substantially different from each other and did not correlate. The labeling by PRPs also did not show correlation with abundance of HDAC proteins in cells. Both the PRP chemotype and the cell type were key in defining which HDAC isoforms were labeled. This is the first report of a cell-permeable uniform set of HDAC PRPs based on different HDACi chemotypes to probe the engagement of multiple HDAC isoforms in live cells and tissues. Further extension of these studies to other types of cells and animal tissues as well as identification of the mechanisms responsible for the modulation of HDACi selectivity and target engagement are in progress.

Experimental Section

1. Biochemical and biological procedures

1.1. Fluorogenic enzymatic assays for class I HDAC isoforms: Human recombinant HDAC1, HDAC2, HDAC3 (BPS Bioscience) and HDAC8 (in-house purified from *E. coli*) were diluted with assay buffer 1 (25 mM Tris·HCl, pH 8.0, 137 mM NaCl, 2.7 mM KCl, and 1 mM $MgCl_2$, 1 mg mL^{-1} BSA) to give 4, 5, 1, and 8.5 ng μL^{-1} stocks of each isoform, respectively. Serial dilutions of the compounds/PRPs were made in assay buffer 2 (25 mM Tris·HCl, pH 8.0, 137 mM NaCl, 2.7 mM KCl, and 1 mM $MgCl_2$) starting with the highest concentration at 1 mM. The enzyme stock (10 μL) and 30 μL of each of the serial dilutions were mixed in a black half-area, low protein

binding 96-well plate (Corning) and pre-incubated for 5 min (3 h for the *o*-aminoanilide derivatives, **6**, **13** and **14**) at room temperature (RT). Next, 10 μL of 125 μM Boc-L-Lys(Ac)-AMC (BLA) fluorescent substrate (Chem-Implex) for HDACs 1–3 or 10 μL of 25 μM Fluor de Lys®, BML-KI178 (Enzo Life Sciences) for HDAC8 was added to each well and incubated for 30 min at RT. The reaction was quenched by the addition of 50 μL of 1 mg mL^{-1} trypsin and 5 μM TSA in assay buffer 2 and incubated for an additional 30 min. The fluorescence signal was read at excitation wavelength 360 nm and emission wavelength 460 nm using a Synergy 4 hybrid microplate reader from BioTek. The statistical data analysis and IC_{50} values were determined using GraphPad Prism 7.02.

1.2. Fluorogenic enzymatic assay for HDAC4: HDAC4 inhibitory activity was determined using the fluorogenic HDAC4 assay kit (BPS Bioscience, catalogue #50064) according to the manufacturer's procedure. The statistical data analysis and IC_{50} values were determined using GraphPad Prism 7.02.

1.3. Cell culture: The human megakaryoblastic cell line SET-2 was cultured in RPMI 1640 medium (Corning, VA, USA) supplemented with 10% heat-inactivated fetal bovine serum (FBS; Sigma–Aldrich, St. Louis, MO, USA). Cells were seeded at a density of 1×10^5 mL^{-1} of medium and were grown at 37 °C with 5% CO_2. Cells were harvested after 72 h, collected by centrifugation, washed, and viability was tested by trypan blue dye exclusion. Collected cells were then resuspended in RPMI 1640 supplemented with 10% heat-inactivated fetal calf serum. A total of 30×10^6 cells was spun down at 500×*g* for 10 min at 4 °C, resuspended in 12 mL PBS and aliquoted into 0.5 mL on a 12-well plate for photolabeling experiments.

Human hepatocellular carcinoma HepG2 or HuH7 cells or human embryonic kidney HEK293T cells were plated in six-well plates (0.5×10^6 cells per well) and grown to 80% confluence in 2 mL culture medium (RPMI 1640 supplemented with 10% FBS, penicillin–streptomycin, and nonessential amino acids) in a humidified atmosphere containing 5% CO_2 at 37 °C. The medium was replaced with 1 mL PBS right before photolabeling experiments.

1.4. Cell-based photolabeling: Cells were pretreated with 200 μM competitor for 15 min (or 3 h for **5** and **6**) where applicable and then treated with 20 μM PRP or DMSO control. After incubation with the PRP at 37 °C for 30 min (or 3 h for PRPs **13** and **14**), the cells were cooled on ice and irradiated with 366 nm light for 30 min. The medium was removed, and the cells gently washed twice with 2 mL PBS and then covered with 1 mL PBS. Cells were scraped/transferred from the plate into Eppendorf tubes, spun down at 1000×*g* for 5 min at 4 °C, the supernatant removed, and the cells resuspended in whole-cell lysis buffer (50 mM HEPES (pH 7.5), 150 mM NaCl, 1% Igepal CA-630, 5% glycerol and 1× protease inhibitor cocktail (Roche)) and 1× phosphatase inhibitor cocktail (ThermoFisher)). Samples were homogenized by vortexing, incubated on a rotating stand at 4 °C for 1 h, then spun down at 19000×*g* for 10 min at 4 °C, and the protein concentrations were determined by bicinchoninic acid (BCA) assay. Next, 35 μg total lysates were incubated with IRDye® 800CW Azide Infrared dye (LI-COR biosciences, part number 926-68070) at a concentration equal to that of the PRP, TCEP (1 mM), TBTA (0.1 mM), and $CuSO_4$ (1 mM) for 90 min at RT. The samples were then frozen at −20 °C until analysis by western blot.

1.5. Mouse tissue photolabeling: A 129/SV mouse was exsanguinated by retro-orbital bleeding, sacrificed, and fresh liver tissue (~ 20 mg) was harvested and immediately homogenized in an Eppendorf tube (using a Teflon homogenizer) containing 500 μL PBS. The tissue homogenate was centrifuged at 13000×*g* for 5 min at 4 °C. The supernatant was discarded, and the cells were resuspended with 1 mL PBS and then centrifuged again at 13000×*g* for 5 min at 4 °C. The cells were resuspended in 1 mL PBS and plated in a six-well plate at a 1:10 dilution. Cells were treated with either DMSO, 10 μM PRP, or 200 μM SAHA then 10 μM PRP in PBS in a humidified atmosphere containing 5% CO_2 at 37 °C (all treatments were done on cells from the same tissue preparation) for 40 min. Cells were then irradiated with UV light (366 nm) for 30 min on ice, harvested by centrifugation at 13000×*g* for 5 min at 4 °C, washed with 1 mL PBS and re-pelleted. The cells were lysed by the addition of 100 μL cold lysis buffer (150 mM NaCl, 50 mM HEPES, 1% Igepal, 5% glycerol, 1× PIC, 1× phosphatase inhibitor cocktail), homogenized by vortexing for 10 s at RT and placed on a rotating stand overnight at 4 °C. The lysate was clarified by centrifugation at 19000×*g* for 10 min at 4 °C. Protein concentration was determined using BCA assay and diluted to 2 mg mL^{-1}; 35 μg of each lysate was reacted with a 0.1 mM azide–PEG3–biotin conjugate (Sigma–Aldrich 762024; 1.7 mM stock in 1:4 DMSO/*t*-butanol) in the presence of 1 mM $CuSO_4$, 0.1 mM TBTA, and 1 mM TCEP for 90 min at RT. The reactions were then stored at −20 °C overnight. Precipitated proteins were pelleted at 6000×*g* for 5 min at 4 °C. Proteins were washed with 250 μL methanol by brief sonication and re-pelleted, then resuspended in PBS containing 0.2% SDS by brief sonication. Proteins were then separated by SDS-PAGE and transferred to a nitrocellulose membrane (as per section 1.7. below). The membrane was blocked and incubated with IRDye® 800CW streptavidin (LI-COR biosciences product number: 926-32230), and labeled protein signal was recorded with an Odyssey Sa scanner at 800 nm. Immunoblotting with HDAC-specific antibodies was done as per section 1.7.

1.6. Photolabeling of recombinant proteins: Recombinant HDAC1 (200 ng) in 10 μL whole-cell lysis buffer (as per section 1.4. above) was pretreated with 100 mM SAHA (**1**) or **S20** or DMSO control for 15 min and then treated with PRP **8** (10 mM) or DMSO control for 40 min. Samples were cooled on ice and irradiated with 366 nm light for 30 min then incubated with 0.1 mM azide–PEG3–biotin conjugate (Sigma–Aldrich 762024; 2.5 mM stock in DMSO) in the presence of 1 mM $CuSO_4$, 0.1 mM TBTA, 1 mM TCEP for 90 min at RT. Samples were then diluted with loading buffer, separated by SDS-PAGE and transferred to nitrocellulose membrane (as per section 1.7. below). The membrane was blocked and incubated with IRDye® 800CW streptavidin, and labeled protein signal was recorded with an Odyssey Sa scanner at 800 nm. Immunoblotting with HDAC-specific antibodies was done as per section 1.7.

1.7. Western blot: Samples containing 30 μg protein were diluted with 4× LDS sample buffer containing DTT (Invitrogen), boiled for 5 min and separated by gel electrophoresis at 100 V. Gels were transferred to nitrocellulose membranes with an iBlot2 transfer system (P3 for 7 min) and visualized with an Odyssey Sa imager at 800 nm. Membranes were then blocked with Odyssey blocking buffer for 2 h at RT or overnight at 4 °C. The blots were incubated with desired antibodies (anti-HDAC1 (Abcam, ab7028), anti-HDAC2 (Abcam, ab12169), anti-HDAC3 (Abcam, ab7030), anti-HDAC8 (Abcam, ab187139), and anti-HDAC4,5,9 (Abcam, ab131524)) at the recommended dilutions for each in Odyssey blocking buffer (LI-COR biosciences, part number: 927-40000) overnight at 4 °C. The blots were then washed 3×5 min with PBST, incubated with relevant species of IRDye® 680RD secondary antibody (LI-COR biosciences, part number: 926-68071) for 1 h and visualized with an Odyssey Sa imager at both 700 and 800 nm. If additional antibody probing was necessary, membranes were stripped with 0.2 N NaOH for 10 min and re-blocked with Odyssey blocking buffer.

1.8. Ethics statement: All animal experiments were approved by the Institutional Animal Care and Use Committee (IACUC) and were performed according to institutional guidelines with approval from the University of Illinois at Chicago Institutional Biosafety and Animal Care Committee (ACC Number: 17-012). All animal procedures were performed in the College of Medicine Research Building at the University of Illinois at Chicago and adhere to the policies of the NIH Office of Laboratory Animal Welfare (OLAW), the standards of the Animal Welfare Act, the Public Health Service Policy, and the Guide for the Care and Use of Laboratory Animals.

2. General chemistry methods

All reagents and solvents were obtained from commercial sources and were used without further purification. Reactions were performed under an inert atmosphere (nitrogen or argon) whenever anhydrous solvents were used. Reactions were monitored by thin-layer chromatography (TLC) using Merck 60 F_{254} silica gel plates or by LC–MS on a Shimadzu LCMS-2020 instrument with either a Waters XSelect HSS CYANO 3.6 μm column or an Agilent XBD-C_{18} 3.5 μm column; dimensions 2.1×20 mm and UV detector at 254 нм. Chromatographic purification was performed on a Biotage Isolera Four instrument using prefilled KP-Sil (normal phase) and KP-C18-HS (reversed phase) SNAP cartridges with UV detection at 254 and 280 nm. ^{1}H, ^{13}C, and ^{19}F NMR spectra were recorded on Bruker spectrometers at 400, 100 and 376 MHz, respectively. Chemical shifts were reported on the δ scale in ppm with the deuterated solvent indicated as the internal reference. Coupling constants are reported in Hz and the standard abbreviations indicating multiplicity were used as follows: s = singlet, bs = broad singlet, d = doublet, t = triplet, q = quartet, and m = multiplet. High-resolution mass spectrometry (HRMS) experiments were performed at either the Mass Spectrometry, Metabolomics and Proteomics Facility at the University of Illinois at Chicago, or at the Mass Spectrometry Laboratory at the University of Illinois at Urbana Champaign on either a Thermo Finnigan LTQ FT ICR Hybrid mass spectrometer, a Shimadzu LCMS IT-TOF mass spectrometer, or a Synapt G2-Si mass spectrometer.

3. Docking, synthetic procedures, and compound characterization

Detailed descriptions of molecular docking, synthetic procedures, and compound characterization are given in the Supporting Information.

Acknowledgements

This study was funded by US National Cancer Institute/National Institutes of Health (NCI/NIH) grants R01 CA131970 and R21 CA183627 (to P.A.P.), National Heart, Lung, and Blood Institute (NHLBI)/NIH grant R01 HL130760 (to N.M.), National Institute of Allergy and Infectious Diseases (NIAID)/NIH grant R01 AI125401 (to A.M.), Alzheimer's Drug Discovery Foundation grant ADDF #20101103 (to P.A.P.), the PhRMA Foundation Fellowship for Pharmacology and Toxicology (to T.Y.T.), and Egyptian Government scholarship JS-2971 (to S.A.).

Conflict of interest

The authors declare no conflict of interest.

Keywords: histone deacetylase · inhibitors · photoaffinity labeling · target engagement · tissue labeling

[1] K. J. Falkenberg, R. W. Johnstone, *Nat. Rev. Drug Discovery* **2014**, *13*, 673–691.

[2] a) O. M. Dovey, C. T. Foster, S. M. Cowley, *Proc. Natl. Acad. Sci. USA* **2010**, *107*, 8242–8247; b) M. Haberland, R. L. Montgomery, E. N. Olson, *Nat. Rev. Genet.* **2009**, *10*, 32–42; c) M. A. Deardorff, M. Bando, R. Nakato, E. Watrin, T. Itoh, M. Minamino, K. Saitoh, M. Komata, Y. Katou, D. Clark, K. E. Cole, E. De Baere, C. Decroos, N. Di Donato, S. Ernst, L. J. Francey, Y. Gyftodimou, K. Hirashima, M. Hullings, Y. Ishikawa, C. Jaulin, M. Kaur, T. Kiyono, P. M. Lombardi, L. Magnaghi-Jaulin, G. R. Mortier, N. Nozaki, M. B. Petersen, H. Seimiya, V. M. Siu, Y. Suzuki, K. Takagaki, J. J. Wilde, P. J. Willems, C. Prigent, G. Gillessen-Kaesbach, D. W. Christianson, F. J. Kaiser, L. G. Jackson, T. Hirota, I. D. Krantz, K. Shirahige, *Nature* **2012**, *489*, 313–317; d) S. Bhaskara, S. K. Knutson, G. Jiang, M. B. Chandrasekharan, A. J. Wilson, S. Zheng, A. Yenamandra, K. Locke, J.-l. Yuan, A. R. Bonine-Summers, C. E. Wells, J. F. Kaiser, M. K. Washington, Z. Zhao, F. F. Wagner, Z.-W. Sun, F. Xia, E. B. Holson, D. Khabele, S. W. Hiebert, *Cancer Cell* **2010**, *18*, 436–447.

[3] a) F. Thaler, C. Mercurio, *ChemMedChem* **2014**, *9*, 523–526; b) A. V. Bieliauskas, M. K. Pflum, *Chem. Soc. Rev.* **2008**, *37*, 1402–1413.

[4] a) Y. Zhang, H. H. Ng, H. Erdjument-Bromage, P. Tempst, A. Bird, D. Reinberg, *Genes Dev.* **1999**, *13*, 1924–1935; b) A. You, J. K. Tong, C. M. Grozinger, S. L. Schreiber, *Proc. Natl. Acad. Sci. USA* **2001**, *98*, 1454–1458; c) L. Alland, R. Muhle, H. Hou, Jr., J. Potes, L. Chin, N. Schreiber-Agus, R. A. DePinho, *Nature* **1997**, *387*, 49–55; d) C. V. Segré, S. Chiocca, *J. Biomed. Biotechnol.* **2011**, *2011*, 690848; e) G. H. Eom, H. Kook, *Pharmacol. Ther.* **2014**, *143*, 168–180; f) J. M. Sun, H. Y. Chen, J. R. Davie, *J. Biol. Chem.* **2007**, *282*, 33227–33236; g) M. K. Pflum, J. K. Tong, W. S. Lane, S. L. Schreiber, *J. Biol. Chem.* **2001**, *276*, 47733–47741; h) Y. Qiu, Y. Zhao, M. Becker, S. John, B. S. Parekh, S. Huang, A. Hendarwanto, E. D. Martinez, Y. Chen, H. Lu, N. L. Adkins, D. A. Stavreva, M. Wiench, P. T. Georgel, R. L. Schiltz, G. L. Hager, *Mol. Cell* **2006**, *22*, 669–679; i) X. Zhang, Y. Ozawa, H. Lee, Y. D. Wen, T. H. Tan, B. E. Wadzinski, E. Seto, *Genes Dev.* **2005**, *19*, 827–839; j) M. G. Guenther, O. Barak, M. A. Lazar, *Mol. Cell. Biol.* **2001**, *21*, 6091–6101.

[5] a) A. K. Adikesavan, S. Karmakar, P. Pardo, L. Wang, S. Liu, W. Li, C. L. Smith, *Mol. Cell. Biol.* **2014**, *34*, 1246–1261; b) J. Frasor, J. M. Danes, C. C. Funk, B. S. Katzenellenbogen, *Proc. Natl. Acad. Sci. USA* **2005**, *102*, 13153–13157; c) A. R. Green, C. Burney, C. J. Granger, E. C. Paish, S. El-Sheikh, E. A. Rakha, D. G. Powe, R. D. Macmillan, I. O. Ellis, E. Stylianou, *Breast Cancer Res. Treat.* **2008**, *110*, 427–437; d) C. L. Smith, I. Migliaccio, V. Chaubal, M. F. Wu, M. C. Pace, R. Hartmaier, S. Jiang, D. P. Edwards, M. C. Gutierrez, S. G. Hilsenbeck, S. Oesterreich, *Breast Cancer Res. Treat.* **2012**, *136*, 253–265.

[6] a) M. Bantscheff, C. Hopf, M. M. Savitski, A. Dittmann, P. Grandi, A. M. Michon, J. Schlegl, Y. Abraham, I. Becher, G. Bergamini, M. Boesche, M. Delling, B. Dumpelfeld, D. Eberhard, C. Huthmacher, T. Mathieson, D. Poeckel, V. Reader, K. Strunk, G. Sweetman, U. Kruse, G. Neubauer, N. G. Ramsden, G. Drewes, *Nat. Biotechnol.* **2011**, *29*, 255–265; b) M. B. Robers, M. L. Dart, C. C. Woodroofe, C. A. Zimprich, T. A. Kirkland, T. Machleidt, K. R. Kupcho, S. Levin, J. R. Hartnett, K. Zimmerman, A. L. Niles, R. F. Ohana, D. L. Daniels, M. Slater, M. G. Wood, M. Cong, Y. Q. Cheng, K. V. Wood, *Nat. Commun.* **2015**, *6*, 10091; c) C. M. Salisbury, B. F. Cravatt, *Proc. Natl. Acad. Sci. USA* **2007**, *104*, 1171–1176; d) H. Y. Kuo, T. A. DeLuca, W. M. Miller, M. Mrksich, *Anal. Chem.* **2013**, *85*, 10635–10642; e) G. Padige, A. T. Negmeldin, M. K. Pflum, *J. Biomol. Screening* **2015**, *20*, 1277–1285; f) T. W. Hanigan, S. M. Aboukhatwa, T. Y. Taha, J. Frasor, P. A. Petukhov, *Cell Chem. Biol.* **2017**, *24*, 1356–1367.

[7] C. M. Salisbury, B. F. Cravatt, *J. Am. Chem. Soc.* **2008**, *130*, 2184–2194.

[8] V. E. Albrow, R. L. Grimley, J. Clulow, C. R. Rose, J. Sun, J. S. Warmus, E. W. Tate, L. H. Jones, R. I. Storer, *Mol. Biosyst.* **2016**, *12*, 1781–1789.

[9] a) B. He, S. Velaparthi, G. Pieffet, C. Pennington, A. Mahesh, D. L. Holzle, M. Brunsteiner, R. van Breemen, S. Y. Blond, P. A. Petukhov, *J. Med. Chem.* **2009**, *52*, 7003 – 7013; b) H. Abdelkarim, M. Brunsteiner, R. Neelarapu, H. Bai, A. Madriaga, R. B. van Breemen, S. Y. Blond, V. Gaponenko, P. A. Petukhov, *ACS Chem. Biol.* **2013**, *8*, 2538 – 2549.

[10] S. A. Fleming, *Tetrahedron* **1995**, *51*, 12479 – 12520.

[11] K. Schnapp, R. Poe, E. Leyva, N. Soundararajan, M. S. Platz, *Bioconjugate Chem.* **1993**, *4*, 172 – 177.

[12] P. A. Marks, R. Breslow, *Nat. Biotechnol.* **2007**, *25*, 84 – 90.

[13] M. Brunsteiner, P. A. Petukhov, *J. Mol. Model.* **2012**, *18*, 3927 – 3939.

[14] S. W. Remiszewski, L. C. Sambucetti, K. W. Bair, J. Bontempo, D. Cesarz, N. Chandramouli, R. Chen, M. Cheung, S. Cornell-Kennon, K. Dean, G. Diamantidis, D. France, M. A. Green, K. L. Howell, R. Kashi, P. Kwon, P. Lassota, M. S. Martin, Y. Mou, L. B. Perez, S. Sharma, T. Smith, E. Sorensen, F. Taplin, N. Trogani, R. Versace, H. Walker, S. Weltchek-Engler, A. Wood, A. Wu, P. Atadja, *J. Med. Chem.* **2003**, *46*, 4609.

[15] S. Balasubramanian, J. Ramos, W. Luo, M. Sirisawad, E. Verner, J. J. Buggy, *Leukemia* **2008**, *22*, 1026 – 1034.

[16] C. J. Chou, D. Herman, J. M. Gottesfeld, *J. Biol. Chem.* **2008**, *283*, 35402 – 35409.

[17] M. Lobera, K. P. Madauss, D. T. Pohlhaus, Q. G. Wright, M. Trocha, D. R. Schmidt, E. Baloglu, R. P. Trump, M. S. Head, G. A. Hofmann, M. Murray-Thompson, B. Schwartz, S. Chakravorty, Z. Wu, P. K. Mander, L. Kruidenier, R. A. Reid, W. Burkhart, B. J. Turunen, J. X. Rong, C. Wagner, M. B. Moyer, C. Wells, X. Hong, J. T. Moore, J. D. Williams, D. Soler, S. Ghosh, M. A. Nolan, *Nat. Chem. Biol.* **2013**, *9*, 319 – 325.

[18] L. Qin, C. Sheridan, J. Gao, *Org. Lett.* **2012**, *14*, 528 – 531.

[19] S. M. Yang, B. Lagu, L. J. Wilson, *J. Org. Chem.* **2007**, *72*, 8123 – 8126.

[20] M. Beconi, O. Aziz, K. Matthews, L. Moumne, C. O'Connell, D. Yates, S. Clifton, H. Pett, J. Vann, L. Crowley, A. F. Haughan, D. L. Smith, B. Woodman, G. P. Bates, F. Brookfield, R. W. Burli, G. McAllister, C. Dominguez, I. Munoz-Sanjuan, V. Beaumont, *PLoS One* **2012**, *7*, e44498.

[21] R. Neelarapu, D. L. Holzle, S. Velaparthi, H. Bai, M. Brunsteiner, S. Y. Blond, P. A. Petukhov, *J. Med. Chem.* **2011**, *54*, 4350 – 4364.

[22] D. P. Dowling, S. G. Gattis, C. A. Fierke, D. W. Christianson, *Biochemistry* **2010**, *49*, 5048 – 5056.

[23] S. Li, G. Fossati, C. Marchetti, D. Modena, P. Pozzi, L. L. Reznikov, M. L. Moras, T. Azam, A. Abbate, P. Mascagni, C. A. Dinarello, *J. Biol. Chem.* **2015**, *290*, 2368 – 2378.

[24] B. E. Lauffer, R. Mintzer, R. Fong, S. Mukund, C. Tam, I. Zilberleyb, B. Flicke, A. Ritscher, G. Fedorowicz, R. Vallero, D. F. Ortwine, J. Gunzner, Z. Modrusan, L. Neumann, C. M. Koth, P. J. Lupardus, J. S. Kaminker, C. E. Heise, P. Steiner, *J. Biol. Chem.* **2013**, *288*, 26926 – 26943.

[25] a) R. R. Rosato, J. A. Almenara, S. Grant, *Cancer Res.* **2003**, *63*, 3637 – 3645; b) N. Fortunati, F. Marano, A. Bandino, R. Frairia, M. G. Catalano, G. Boccuzzi, *Int. J. Oncol.* **2014**, *44*, 700 – 708; c) M. Tavakoli-Yaraki, F. Karami-Tehrani, V. Salimi, M. Sirati-Sabet, *Tumour Biol.* **2013**, *34*, 241 – 249.

[26] W. K. Kelly, O. A. O'Connor, L. M. Krug, J. H. Chiao, M. Heaney, T. Curley, B. MacGregore-Cortelli, W. Tong, J. P. Secrist, L. Schwartz, S. Richardson, E. Chu, S. Olgac, P. A. Marks, H. Scher, V. M. Richon, *J. Clin. Oncol.* **2005**, *23*, 3923 – 3931.

[27] J. H. Noh, H. J. Bae, J. W. Eun, Q. Shen, S. J. Park, H. S. Kim, B. Nam, W. C. Shin, E. K. Lee, K. Lee, J. J. Jang, W. S. Park, J. Y. Lee, S. W. Nam, *Cancer Res.* **2014**, *74*, 1728 – 1738.

[28] a) R. Brunmeir, S. Lagger, C. Seiser, *Int. J. Dev. Biol.* **2009**, *53*, 275 – 289; b) S. Chen, X. Yao, Y. Li, Z. Saifudeen, D. Bachvarov, S. S. El-Dahr, *Development* **2015**, *142*, 1180 – 1192; c) P. Somanath, R. Herndon Klein, P. S. Knoepfler, *PLoS One* **2017**, *12*, e0185627.

[29] a) A. S. Vaidya, B. Karumudi, E. Mendonca, A. Madriaga, H. Abdelkarim, R. B. van Breemen, P. A. Petukhov, *Bioorg. Med. Chem. Lett.* **2012**, *22*, 5025 – 5030; b) A. M. Kral, N. Ozerova, J. Close, J. Jung, M. Chenard, J. Fleming, B. B. Haines, P. Harrington, J. Maclean, T. A. Miller, P. Secrist, H. Wang, R. W. Heidebrecht, Jr., *Biochemistry* **2014**, *53*, 725 – 734.

[30] T. Eckschlager, J. Plch, M. Stiborova, J. Hrabeta, *Int. J. Mol. Sci.* **2017**, *18*, 1414.

Manuscript received: February 20, 2019
Revised manuscript received: March 28, 2019
Accepted manuscript online: March 28, 2019
Version of record online: April 10, 2019